Chinese Chemical Letters 33 (2022) 1488–1492

Contents lists available at ScienceDirect

Chinese Chemical Letters

journal homepage: www.elsevier.com/locate/cclet

Chirality and chiral functional composites of bicontinuous cubic nanostructured cubosomes

Deyin Wang, Hongkai Liu, Wei Wang*

Center for Synthetic Soft Materials, Key Laboratory of Functional Polymer Materials of Ministry of Education and Institute of Polymer Chemistry, College of Chemistry, Nankai University, Tianjin 300071, China

ARTICLE INFO

Article history:
Received 1 May 2021
Revised 7 August 2021
Accepted 8 August 2021
Available online 12 August 2021

Keywords:
Chirality
Self-assembly
Nanostructure
Composite

ABSTRACT

Molecular self-assembly is the most important strategy for the development of chiral aggregates and chiral functional materials. In this study, we rationally designed and synthesized chiral fluorescent heteroclusters that were self-assembled into microscale cubosomes with a three-dimensional (3D) bicontinuous cubic phase nanostructure. The cubosomes exhibited chirality, indicating that chirality is transferred from the molecules to the 3D nanostructure. Therefore, we confirmed the formation of a chiral bicontinuous cubic phase nanostructure for the first time. We also showed that this chirality originates from the continuous change in the saddle-splay distortion of the molecules within the curved bilayer. At the same time, transparent films of chiral composites were prepared by mixing the chiral cubosomes with an epoxy resin and then curing the mixture. Therefore, we demonstrated an effective method for preparing chiral composites.

Lipids are biological molecules composed of a hydrophilic head group and hydrophobic fatty acid tails. Their amphiphilic nature allows them to self-assemble into nano-objects or nanostructures, such as micelles, and vesicles, and complex three-dimensional (3D) bicontinuous cubic networks through intermolecular noncovalent interactions [1]. Experimental and theoretical studies [1–8] on the self-assembly principle of lipids provide guidance not only on the formation of complex biological nanostructures, such as biophotonic crystals with 3D cubic networks [9–12], but also on their applications in the fabrication of advanced materials with 3D cubic nanostructures, such as artificial photonic crystals for metamaterials [13,14] and nanoporous particles [15,16] for catalyst supports [17] and controlled drug release [18].

The self-assembly principle of lipids has been also used to develop self-assembled systems with supramolecular chirality [19–23] and supramolecular chiral functional materials [24,25]. Through rational molecular design, chiral building blocks self-assemble into *quasi*-one-dimensional supramolecular aggregates, such as twisted or helical ribbons, and nanotubes. These supramolecular aggregates usually exhibit left- or right-handed superstructures, in which the molecules are persistently twisted along the axis of the aggregate. In this way, the chirality of the molecules is transferred to the supramolecular chirality through self-assembly.

Studies on the chirality of self-assembled systems with a 3D bicontinuous cubic structures are extremely limited. Chiral bicontinuous cubic structures were first observed in the lyotropic liquid phase of two chiral lipids in water [26,27]. Recently, they were found in thermotropic bicontinuous cubic phases of bolaamphiphiles and rod molecules [28–30]. This work aimed to further study chirality of 3D bicontinuous cubic structures. In our previous studies, we designed and subsequently synthesized a series of the dumbbell-shaped Janus heteroclusters composed of a polyoxometalate (POM) cluster, a polyhedral oligomeric silsesquioxane (POSS), and different organic linkers [31–34]. These heteroclusters then self-assembled into cubosomes with a bicontinuous double diamond (DD) cubic nanostructure in solution [34]. In this study, we inserted the L- and D-enantiomers of a chiral amino acid and a fluorescent naphthalene dianhydride into the organic linkers of the heteroclusters, which were then self-assembled them into cubosomes. These cubosomes were confirmed to have the DD cubic nanostructure by scanning and transmission electron microscopy (SEM and TEM) and small-angle X-ray scattering (SAXS) analysis. The chirality of the cubosomes were characterized by circular dichroism (CD) spectroscopy. We discussed the correlation between molecular chirality and the chirality of the DD cubic nanostructure constructed by non-twisted or non-helical self-assembled bilayers. In addition, chiral functional composites were also pre-

* Corresponding author.
E-mail address: weiwang@nankai.edu.cn (W. Wang).

https://doi.org/10.1016/j.cclet.2021.08.040
1001-8417/

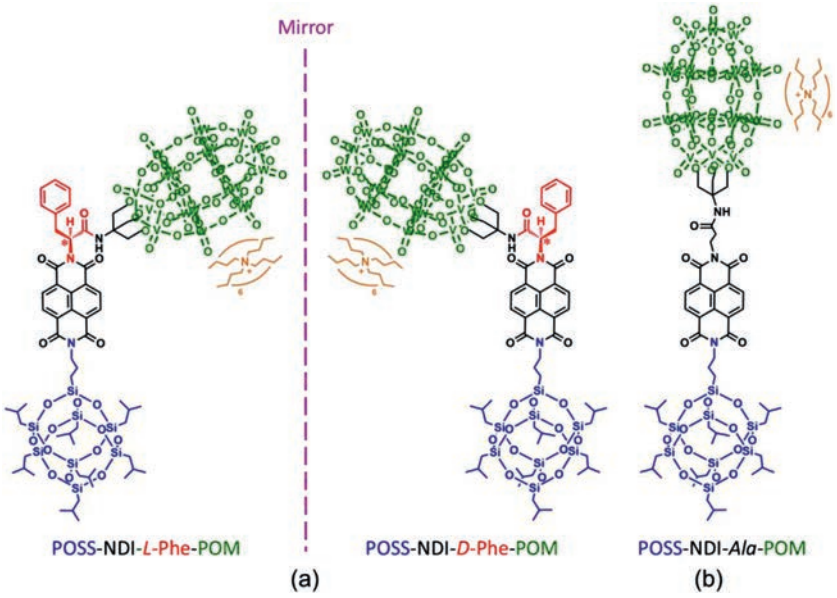

Fig. 1. Chemical structures of (a) chiral heteroclusters in L- and D-forms and (b) an achiral heterocluster. The organic linkers between the polyoxometalate (POM) and polyhedral oligomeric silsesquioxane (POSS) clusters are composed of 1,4,5,8-naphthalenetetracarboxylic dianhydride (NDI) and L- or D-phenylalanine or β-alanine.

pared by curing mixtures of chiral cubosomes and an epoxy resin.

Fig. 1 shows the chemical structures of the heteroclusters used in this study. The formulas and molecular weights are $(Bu_4N)_6H_3(P_2W_{15}V_3O_{62})$, 5422.2 Da for the POM cluster and $C_{31}H_{71}Si_8O_{12}$, 874.6 Da for 1-aminopropyl-3,5,7,9,11,13,15-heptaisobutyl POSS. To endow them with molecular chirality, we inserted a chiral unit, specifically, an enantiomer of the α-amino acid, that is, L- and D-phenylalanine (L- and D-Phe) into the organic linker. Concurrently, we added 1,4,5,8-naphthalenetetracarboxylic dianhydride (NDI) as a light-absorbing group to the organic linker for the detection of the chirality of the self-assembled cubosomes by CD spectroscopy. The dumbbell-shaped enantiomers are designated as POSS-NDI-L-Phe-POM (or L-heterocluster) and POSS-NDI-D-Phe-POM (or D-heterocluster), as shown in Fig. 1a. The specific optical rotations of L- and D-heteroclusters are $[\alpha]_D^{20} + 8.0^\circ$ and $[\alpha]_D^{20} - 8.0^\circ$, we also prepared an achiral heterocluster in which phenylalanine is substituted by β-alanine, denoted as POSS-NDI-Ala-POM (or Ala-heterocluster).

The general synthetic route for these molecules is the same as that reported in our previous works [31] and the details are available in Supporting information. The experimentally determined molecular weights of L-, D- and Ala-heteroclusters are 6743.10, 6743.19, and 6667.17 Da, respectively, which are the same as the theoretical values (6743.14, 6743.14 and 6667.07 Da). The UV–vis absorption spectra of the three heteroclusters in acetone solution show typical UV–vis absorption peaks at λ = 345, 364 and 384 nm, and the fluorescence emission peaks at λ = 402, 426 and 457 nm, which are the characteristic peaks of the NDI unit (Fig. S1 in Supporting information). We also measured the UV–vis absorption and fluorescence emission spectra of POSS-NDI-L-Phe-COOH (Fig. S2 in Supporting information). The inserted table lists the peak positions of the UV–vis absorption and fluorescence emission spectra of POSS-NDI-L-Phe-COOH and POSS-NDI-L-Phe-POM. Clearly, the spectral differences between POSS-NDI-L-Phe-COOH and POSS-NDI-L-Phe-POM are negligible.

To study the chirality of cubosomes with a bicontinuous DD cubic nanostructure, we implemented the dynamic process used in our previous study [34] for the self-assembly of these newly synthesized heteroclusters. Here, we briefly introduce the self-assembly process. The POM and POSS clusters dissolve well in acetone and *n*-decane, respectively. Therefore, the resulting heteroclusters possess a Janus nature and are well soluble in a 3:2 acetone/*n*-decane mixture (v/v) at room temperature. Because the evaporation of acetone is ~80 times faster than that of *n*-decane (Table S1 in Supporting information), the gradual evaporation of acetone from the mixture increases the proportion of *n*-decane in the mixture, which is a selective solvent for the POSS block. During this process, the L-, D- and Ala-heteroclusters self-assemble into cubosomes, which are referred to as L-, D- and Ala-cubosomes, respectively, for convenience. Under the same condition, we also co-assembled mixtures of the L- and D-heteroclusters with L/D ratios of 25/75, 50/50, and 75/25 (mol/mol) into cubosomes. Hereafter, these cubosomes are referred to as D/L-cubosomes.

To confirm that the heteroclusters form cubosomes with bicontinuous DD cubic nanostructures, we characterized the cubosomes using scanning electron microscopy (SEM), transmission electron microscopy (TEM), and small angle X-ray scattering (SAXS). We observed similar results for all cubosomes formed by self-assembly and co-assembly, as summarized in Figs. S3–S5 (Supporting information). The SEM and TEM images for the L-cubosomes are shown in Fig. 2. The SEM observation shows truncated octahedral cubosomes (Figs. 2a and b) with an average diameter of 1406 ± 288 nm (Figs. 2c). For the TEM characterization, we selected a cubosome with a size less than 400 nm to view the internal nanostructure. The TEM images in Figs. 2d and f exhibit the nanostructure of the bicontinuous DD cubic phase viewed along the [111] and [100] zone axes [34]. In the bright field mode, the dark regions are POM-rich because the POM cluster contains 15 tungsten atoms, while the bright regions are POSS-rich. The close-up images in Fig. 2e and g and the corresponding fast Fourier transform patterns (insets) reveal the symmetry and *d*-spacing of the two projections in reciprocal space: the hexagonal symmetry of the white dots with an observed lattice spacing of d_{111} = 8.6 ± 0.2 nm (Fig. 2d) and the cubic symmetry of the white (or dark) dots with an observed lattice spacing of d_{100} = 7.8 ± 0.2 nm (Fig. 2f).

The SAXS characterization provides the critical evidence of the identity of the inner nanostructure. Fig. 3a is the SAXS spectra of the cubosomes within q = 0.2–2.0 nm^{-1}, where q is the scattering vector. We can identify one strong peak and two to three

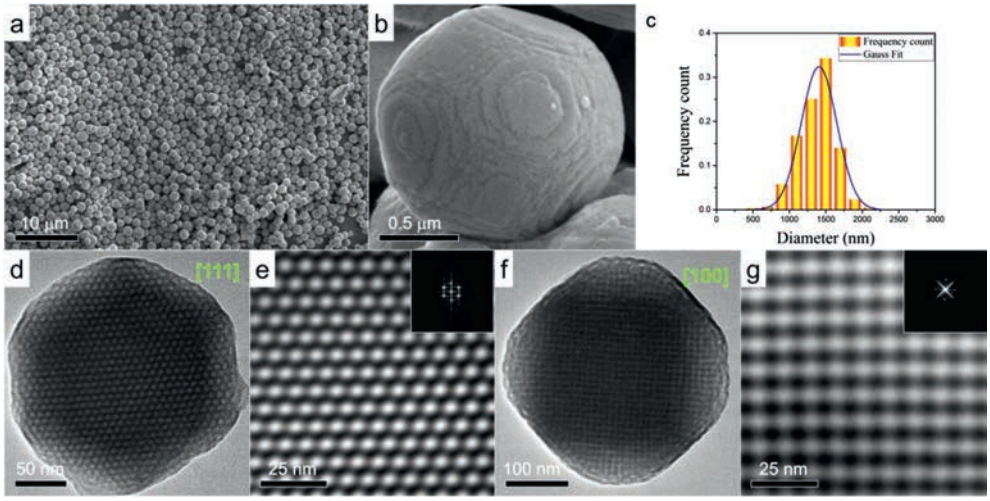

Fig. 2. (a) Low-magnification SEM image of the L-cubosomes. (b) Close-up SEM image of a truncated octahedral cubosome. (c) Size distribution of the L-cubosomes in A. (d) to (g) TEM images of the L-cubosomes and close-up images viewed along the [111], and [100] zone axes of the double diamond structure. The insets are the corresponding fast Fourier transform pattern.

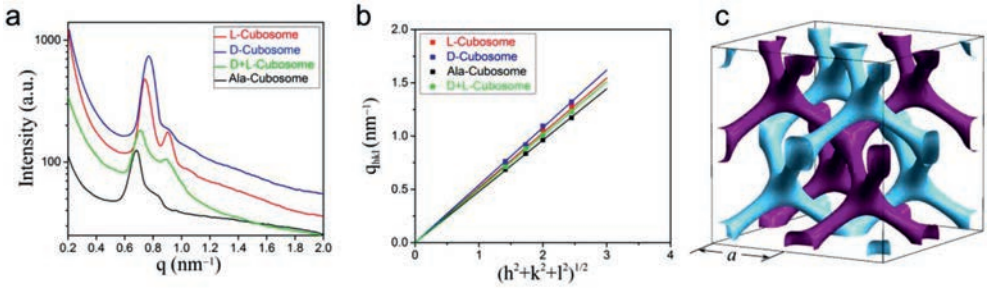

Fig. 3. (a) SAXS spectra of the L-, D-, Ala- and D/L-cubosomes (q is the scattering vector). (b) Linear relationship between q_{hkl} and $(h^2+k^2+l^2)^{1/2}$ (q_{hkl} is the reciprocal spacing of the cubic phase and h, k and l are the Miller indices of the corresponding planes). (c) Skeletal drawing of a cubic unit cell with two sets of diamond nanostructures differentiated by purple and sky-blue colors. Lattice constant a is indicated. For interpretation of the references to color in this figure legend, the reader is referred to the web version of this article.

weak peaks or shoulder peaks from the enlarged SAXS spectra (Fig. S5). The $\sqrt{2}$:$\sqrt{3}$:$\sqrt{4}$:$\sqrt{6}$ spacing ratio of these peaks index them to the [110], [111], [200] and [211] reflections of the bicontinuous DD cubic phase [34–36], indicating the space group of the bicontinuous cubic phase is $Pn\bar{3}m$. The reciprocal spacing q_{hkl} of the cubic phase is associated with lattice constant a by the equation $q_{hkl} = 2\pi\sqrt{h^2+k^2+l^2}/a$, where h, k, and l are the Miller indices. The a values are 12.3, 11.6, and 13.1 nm, respectively, for L-, D- and Ala-cuobsomes, as determined from the slopes of the regression lines passing through the origin (Fig. 3b). On the other hand, a = 11.9, 12.5, and 11.2 nm for the D/L-cubosomes with molar ratios of L/D = 25/75, 50/50 and 75/25 (mol/mol), respectively (Fig. S5). Hence, we conclude that a DD nanostructure formes inside the cubosomes, as shown in Fig. 3c. The drawing of the unit cell depicts the symmetry of the DD structure: 2 equiv. but independent diamonds are constructed by the nodes and channels, which are differentiated by purple and sky-blue colour [34,37].

We studied the chirality of the cubosomes by obtaining their CD spectra of the *n*-decane suspensions with a concentration of 0.5 mg/mL. We examined the following suspensions: (1) L-, D-, and Ala-cubosomes, (2) L/D-cubosomes with L/D ratios of 25/75, 50/50 and 75/25 (mol/mol), (3) mixtures of L-, D-, and Ala-cubosomes with ratios of 25/75, 50/50 and 75/25 (mol/mol), which are referred to as L/D-, L/Ala-, and D/Ala-mixtures, respectively. We also examined the molecular solution of L- and D-heteroclusters in acetone and the *n*-decane suspensions of the L- and D-heterocluster powders that were prepared by rapidly injecting their tetrahydrofuran solutions into the water. Fig. 4a shows the CD signals in the wavelength range from 300 nm to 500 nm. First, the L- and D-cubosomes exhibit Cotton effects in the 350–425 nm region, which are typical of the CD spectra of self-assembled systems containing NDI units and are corresponding with the UV-vis absorption bands of the cubosomes (Fig. S6 in Supporting information). The two spectra are mirror images of each other and show the positive and negative Cotton effects for the D- and L-cubosomes, respectively. Second, depending on the ratio content of the chiral heteroclusters, the absolute intensities of the CD signals of the L/D-cubosomes and the L/D, L/Ala- and D/Ala cubosome mixtures lin-

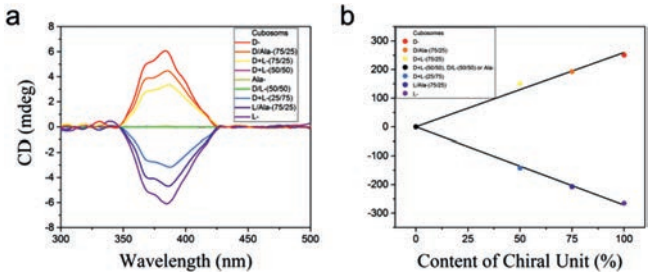

Fig. 4. (a) CD spectra of the cubosomes self-assembled and co-assembled by the heteroclusters and of mixtures of the cubosomes at different ratios in *n*-decane (c = 0.5 mg/mL). The symbols "+"and "/" denote the co-assembly of L- and D-heteroclusters and the mixture of the L- and D-cubosomes, respectively. (b) Linear relationship between the CD intensity and chiral unit content.

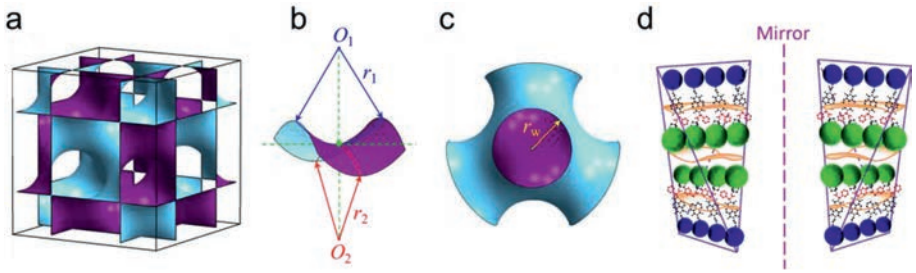

Fig. 5. (a) Cubic unit cell of the double diamond structure described using a minimal surface. (b) Saddle surface of a hyperbolic paraboloid containing a saddle point (green) and r_1 and r_2 as the two principal radii of the curvature. (c) Water channel with a radius (r_w). (d) Suggested mirror arrangement of the chiral L- and D-heteroclusters in bilayer with saddle-splay distortion following Bouligand's drawing [42].

early decreases with increasing net ratio of 50/50 (Fig. 4b). We did not observe the chiral enhancement [38] possibly due to the larger diameters of POM and POSS in the heteroclusters resulting in a large distance between NDI units. Third, the Ala-cubosome suspensions in *n*-decane (Fig. 4a), the acetone solutions of the L- or D-heteroclusters with the concentrations of c = 0.1, 1.0, and 10.0 mg/mL (Fig. S7 in Supporting information), and the *n*-decane suspensions of the L- and D-heterocluster powder (Fig. S8 in Supporting information) do not show any CD signal in the same region. The CD spectra of L- and D-cubosomes with the concentrations of 1.0, 0.5 and 0.25 mg/mL were also tested, and their intensities changed with the concentrations (Fig. S9 in Supporting information). Therefore, we conclude that the CD signals originate from the chiral L- and D-phenylalanine units within the ordered structures of the cubosomes. In other words, the molecular chirality of L- and D-phenylalanine is transferred to cubosomes through the bicontinuous DD cubic structures; thus we consider these structures as chiral bicontinuous DD cubic structures or chiral cubosomes. We also carried out the linear dichroism (LD) studies of the resulting chiral cubosomes. LD spectra of the chiral cubosomes monitored under various angles did not show any obvious signals (Fig. S10 in Supporting information). These observations indicate the suprastructure within the cubosomes plays a key role in the chirality transfer from the molecular to the supramolecular level [39,40].

To the best of our knowledge, there are very few studies on the bicontinuous cubic phases of chiral molecules. There is only one structural study on the bicontinuous cubic phases of two chiral lipids, dihexadecyl phosphatidylethanolamine and didodecyl phosphatidylethanolamine in water by SAXS [26,27]. Unfortunately, the chirality was not directly determined by CD spectrometry, possibly owing to the lack of UV–vis absorption moities in the two lipids. Since then, no follow-up studies have been reported possibly because it is difficult to self-assemble the lipids with a covalently connected chromophore unit into chiral bicontinuous cubic structures. Nevertheless, we believe that the bicontinuous cubic phases are chiral. As mentioned earlier, chiral bicontinuous cubic phases were recently found in thermotropic liquid crystal phases of some rod-like compounds or bolaamphiphiles [28−30], and the temperature dependent CD spectra were also determined from the thermotropic liquid crystal phases of two chiral compounds [28], However, the structures in these bicontinuous cubic phases are different from those formed by lipid bilayers.

It is worth noting that through electron microscopy observation, supramolecular chirality of *quasi*-one-dimensional twisted or helical ribbons and nanotubes is early identifiable, that is, left- or right-handed helices or ribbons [19−21]. However, our SEM and TEM observations show that there are no similar deformed bilayers or structures on the surface, edge, and interior of the L- and D-cubosomes (Fig. 2 and Fig. S11 in Supporting information). Therefore, the chiral cubosomes do not have the appearance of the chiral superstructure that characterizes left- or right-handed ribbons.

Bicontinuous DD cubic structure is a unique network constructed by two independent nanochannels separated by a curved bilayer. Fig. 5a is a triply periodic minimal surface structure showing the lattice of a bicontinuous DD cubic phase. The purple and sky-blue sides of the curved surface distinctly distinguish the two continuous but nonintersecting channel networks. Fig. 5b schematically shows the curved surface with two curvatures $c_1 = 1/r_1$ and $c_2 = 1/r_2$, where r_1 and r_2 are the principal radii of the curvatures. The topological characteristic of the curved surface is that every point is a saddle point with a negative Gaussian curvature ($K = c_1c_2 < 0$) and zero mean curvature [$H = (c_1 + c_2)/2 = 0$] in which c_1 and c_2 are not constant changing from zero to the maximum in a so-called water channel [3,41]. Radius, r_w, of water channel (Fig. 5c) can be calculated according to the equation:

$$r_w = 0.391a - l \quad (1)$$

where a is the lattice constant, and l is the length of the molecule [38]. Taking L-cubosomes as an example, a = 12.3 nm, and l = 3.5 nm, we obtain r_w = 1.31 nm, thus the corresponding curvatures are $c_1 = -c_2 = 0.76$ nm^{-1}.

The molecules in the bilayer at each saddle point suffer from a saddle-splay distortion. According to the widely accepted saddle-splay distortion of lipid bilayers proposed by Bouligand [1,2,42], we hypothesize that the L- and D-heteroclusters are arranged such that the chiral L- and D-phenylalanine enantiomers are nonsuperimposable mirror images of one another (Fig. 5d). We believe that this is the origin of the chirality of the bicontinuous cubic structure. Because the surface curvature is not constant in the bicontinuous cubic structures, the saddle-splay distortion further varies with the point. In other words, the chiral transfer from the molecules to cubosomes varies at each point and consequently, the heterocluster bilayer does not show any left- or right-handed deformation. To confirm this hypothesis, we prepared the planar structures form by the L- and D-heteroclusters. The absence of CD signals for the plates imply the invalid chiral transfer from the heteroclusters to planar structures (Figs. S12 and S13 in Supporting information).

In this study, we further prepared chiral composites by mixing the cubosome powder with an epoxy resin (Fig. S14 in Supporting information) (at a ratio 1:100 by weight) and then curing the mixture. The two optical images in Fig. 6a show the films of a cured pure epoxy resin and composite on a quartz glass. The composite films are slightly yellowish and transparent, allowing the characters under the film to be visible. Relative to that of the pure epoxy film, the transmittance values of the composite films of the L- and D-cubosomes are 86.9% and 82.4%, respectively. We observed several cubosomes on the fracture surface of a composite by SEM (Fig. 6b). We also used SAXS to confirm the bicontinuous DD structures within the cubosomes (Fig. S15 in Supporting information). The CD spectra of the two composite films are the same as those of the L- and D-cubosomes in the 350−425 nm region (Fig. 6c). The

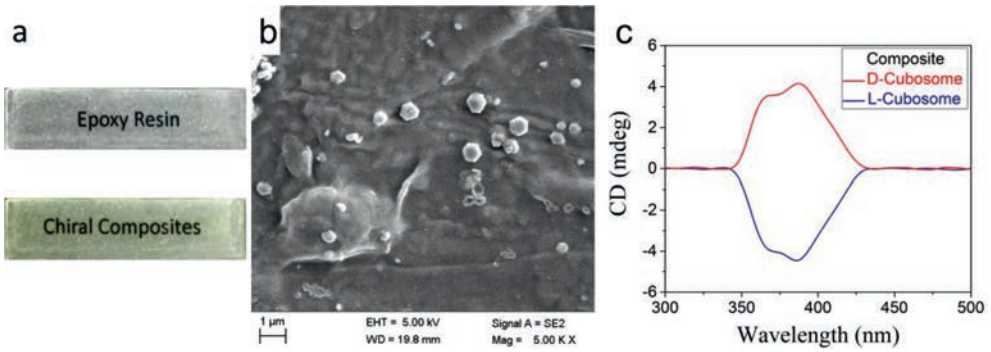

Fig. 6. (a) Two optical images showing films of cured pure epoxy resin and cured composites of the L- or D-cubosome on a quartz plate. (b) SEM image showing a few cubosomes on a fracture surface of a composite. (c) CD spectra of the chiral composites.

chiral composite films have the potential applications in terms of chiral recognition, chiroptical switches, chiral electronics and biology.

In summary, we designed and synthesized three dumbbell-shaped Janus heteroclusters composed of POM and POSS clusters with different organic linkers that contain a fluorescent NDI unit. The L- or D-phenylalanine enantiomer was inserted into the organic linker of two chiral heteroclusters, whereas achiral β-alanine was inserted into that of the achiral heterocluster. These heteroclusters self-assembled into cubosomes with a bicontinuous DD cubic structure. CD characterization revealed that the cubosomes of the chiral heteroclusters exhibit chirality, indicating that chirality is transferred from molecules to the bicontinuous DD cubic structure. Our analysis indicated that the saddle-splay distortion of molecules within curved bilayer of the heteroclusters is the origin of the chirality of the cubic phase nanostructure. We further prepared chiral transparent films of composites by curing mixtures of the chiral cubosomes and an epoxy resin. Therefore, we demonstrated a simple but effective method of preparing chiral functional composites for advanced applications.

Declaration of competing interest

The authors declare that they have no known competing financial interests or personal relationships that could have appeared to influence the work reported in this paper.

Acknowledgments

We thank for the financial support given by the National Natural Science Foundation of China (No. 92061120) and the help of Prof. Yongfeng Men and Dr. Xiao Yang of SAXS at Changchun Institute of Applied Chemistry (CIAC). This paper is also dedicated to the 100th anniversary of Chemistry at Nankai University.

Supplementary materials

Supplementary material associated with this article can be found, in the online version, at doi:10.1016/j.cclet.2021.08.040.

References

[1] J.M. Seddon, R.H. Templer, Polymorphism of lipid-water systems, in: R. Lipowsky, E. Sackmann (Eds.), Handbook of Biological Physics, Elsevier Science, 1995, pp. 97–160.
[2] J.M. Seddon, Biochim. Biophys. Acta Rev. Biomembr. 1031 (1990) 1–69.
[3] C.V. Kulkarni, W. Wachter, G. Iglesias-Salto, S. Engelskirchen, S. Ahualli, Phys. Chem. Chem. Phys. 13 (2011) 3004–3021.
[4] L. van't Hag, S.L. Gras, C.E. Conn, C.J. Drummond, Chem. Soc. Rev. 46 (2017) 2705–2731.
[5] J.N. Israelachvili, D.J. Mitchell, B.W. Ninham, J. Chem. Soc. Faraday Trans. 2 72 (1976) 1525–1568.
[6] J.N. Israelachvili, D.J. Mitchell, B.W. Ninham, Biochim. Biophys. Acta Biomembr. 470 (1977) 185–201.
[7] W. Helfrich, Z. Naturforsch. C 28 (1973) 693–703.
[8] S.T. Hyde, B. Ninham, S. Andersson, et al., The Language of Shape, Elsevier, Amsterdam, 1997.
[9] J.W. Galusha, L.R. Richey, J.S. Gardner, J.N. Cha, M.H. Bartl, Phys. Rev. E 77 (2008) 050904 R.
[10] K. Michielsen, D.G. Stavenga, J. R. Soc. Interface 5 (2008) 85–94.
[11] V. Saranathan, C.O. Osuji, S.G.J. Mochrie, et al., Proc. Natl. Acad. Sci. U. S. A. 107 (2010) 11676–11681.
[12] B.D. Wilts, B.A. Zubiri, M.A. Klatt, et al., Sci. Adv. 3 (2017) e1603119.
[13] A.M. Urbas, M. Maldovan, P. DeRege, E.L. Thomas, Adv. Mater. 14 (2002) 1850–1853.
[14] L. Han, S. Che, Adv. Mater. 30 (2018) 1705708.
[15] C.T. Kresge, M.E. Leonowicz, W.J. Roth, J.C. Vartuli, J.S. Beck, Nature 359 (1992) 710–714.
[16] J.S. Beck, J.C. Vartuli, W.J. Roth, et al., J. Am. Chem. Soc. 114 (1992) 10834–10843.
[17] A. Corma, Chem. Rev. 97 (1997) 2373–2420.
[18] F. Tang, L. Li, D. Chen, Adv. Mater. 24 (2012) 1504–1534.
[19] J.J.L.M. Cornelissen, A.E. Rowan, R.J.M. Nolte, N.A.J.M. Sommerdijk, Chem. Rev. 101 (2001) 4039–4070.
[20] T. Shimizu, M. Masuda, H. Minamikawa, Chem. Rev. 105 (2005) 1401–1443.
[21] Themed issue, Chem. Soc. Rev. 38 (2009) 657–852.
[22] M. Liu, L. Zhang, T. Wang, Chem. Rev. 115 (2015) 7304–7397.
[23] J. Wu, W. Liang, T. Niu, et al., Chem. Commun. 54 (2018) 9206–9209.
[24] D.B. Amabilino, J. Veciana, Top. Curr. Chem. 265 (2006) 253–302.
[25] D.Y. Wang, H.K. Liu, W. Wang, Compos. Commun. 27 (2021) 100859.
[26] P. Mariani, V. Luzzati, H. Delacroix, J. Mol. Biol. 204 (1988) 165–189.
[27] J.M. Seddon, J.L. Hogan, N.A. Warrender, E. Pebay-Peyroula, Prog. Colloid Polym. Sci. 81 (1990) 189–197.
[28] C. Dressel, F. Liu, M. Prehm, et al., Angew. Chem. Int. Ed. 53 (2014) 13115–13120.
[29] C. Dressel, T. Reppe, S. Poppe, et al., Adv. Funct. Mater. 30 (2020) 2004353.
[30] X. Zeng, G. Ungar, J. Mater. Chem. C 18 (2020) 5389–5398.
[31] M.B. Hu, Z.Y. Hou, W.Q. Hao, et al., Langmuir 29 (2013) 5714–5722.
[32] H. Wu, Y.Q. Zhang, M.B. Hu, et al., Langmuir 33 (2017) 5283–5290.
[33] H.Y. Wang, L.J. Ren, X.G. Wang, J.B. Ming, W. Wang, Langmuir 35 (2019) 6727–6734.
[34] H.K. Liu, L.J. Ren, H. Wu, et al., J. Am. Chem. Soc. 141 (2019) 831–839.
[35] W. Longley, T.J. McIntosh, Nature 303 (1983) 612–614.
[36] H. Kim, Z. Song, C. Leal, Proc. Natl. Acad. Sci. U. S. A. 114 (2017) 10834–10839.
[37] http://www.msri.org/publications/sgp/jim/models/copolymers/projections/standard/aba111/index.html.2021
[38] M. Pandeeswar, M.B. Avinash, T. Govindaraju, Chem. Eur. J. 18 (2012) 4818–4822.
[39] A. Tsuda, M.D.A. Alam, T. Harada, et al., Angew. Chem. Int. Ed. 46 (2007) 8198–8202.
[40] M. Wolffs, S.J. George, Ž. Tomović, et al., Angew. Chem. Int. Ed. 46 (2007) 8203–8205.
[41] D.M. Anderson, S.M. Gruner, S. Leibler, Proc. Natl. Acad. Sci. U. S. A. 85 (1988) 5364–5368.
[42] Y. Bouligand, J. Phys. Colloq. 51 (1990) C7–35 C7-52.